IEEE Access
Multidisciplinary | Rapid Review | Open Access Journal

Received September 6, 2017, accepted October 13, 2017, date of publication October 18, 2017,
date of current version November 14, 2017.

Digital Object Identifier 10.1109/ACCESS.2017.2764126

No-Reference Quality Assessment of Noise-Distorted Images Based on Frequency Mapping

GUANGYI YANG, YUE LIAO, QINGYI ZHANG, DESHI LI, AND WEN YANG, (Senior Member, IEEE)
School of Electronic Information, Wuhan University, Wuhan 430072, China

Corresponding author: Deshi Li (dsli@whu.edu.cn)

This work was supported in part by the National Natural Science Foundation of China under Grant 61571334 and in part by the National High Technology Research and Development Program (863 Program) under Grant 2014AA09A512.

ABSTRACT In this paper, we propose a no-reference image quality assessment (IQA) metric for noise-distorted images specifically based on frequency mapping (FM), namely, FMIQA index. First, we decompose the image into intrinsic mode functions (IMFs) from small to large scale by using bidimensional empirical mode decomposition (BEMD), and perform the local feature analysis on the IMFs by Riesz transform. Considering that the combination of BEMD and Riesz transform can denoise the noise-distorted image, we use this method with appropriate application of visual contrast sensitivity function to get the denoised image. Then we calculate the similarity map of the Riesz transform feature maps from the distorted image and the denoised image to obtain the similarity indices. Finally, we combine these similarity indices to obtain the final index. Experimental results on three public databases show that the proposed FMIQA evaluates the noise-distorted image in consistency with subjective assessment and can obtain better performance in image quality prediction than other existing related methods.

INDEX TERMS No-reference image quality assessment (NR-IQA), frequency mapping (FM), Riesz transform, bidimensional empirical mode decomposition (BEMD), contrast sensitivity function (CSF).

I. INTRODUCTION

With the booming development of digital technology and multimedia communication, digital images have been widely applied as an important element of information expression and communication [1]. However, during the process of transmission [2], image matching [3], target detection [4], and others [5]–[7], interference such as noise, blur, data loss, etc. will be inevitably introduced, resulting in image quality degradation [8]. How to evaluate the visual distortion generated from these processes is significant for various multimedia applications. Image quality assessment (IQA) research has raised a lot of attention in the past twenty years [9], and there are two different IQA methods of subjective quality assessment [10], [11] and objective quality assessment [12]. Subjective IQA is the most intuitive and reliable method, but it takes a lot of time and labor cost. Consequently, it can not be used in practice [13]. Objective IQA aims at designing a mathematical model to represent the human judgements as precise as possible. The challenge of objective IQA method is how to find out reliable and effective approaches to assess the visual quality of an image [14], [15].

According to the presence or absence of reference images, objective IQA can be divided into Full-Reference (FR), Reduced-Reference (RR), and No-Reference (NR) approaches [16]. FR-IQA metrics are designed based on original images, which are taken as reference images. They are mainly used in assessing the similarity and fidelity between distorted and original images [17]–[20]. FR-IQA metrics can obtain good performance in visual quality prediction, but the disadvantage is that the reference image is necessary, which is often unavailable in practical applications. RR-IQA metrics do not need the complete reference image, but only require part information of the reference image, such as the probability distribution of the wavelet transform coefficients, the integrated multiscale geometric analysis and perceived gray difference features [21], [22]. The corresponding application fields include digital watermark verification in video transmission, video quality monitoring and bit rate control

using sub-channels [23]–[26]. Recently, the study of the NR-IQA has been active because of the difficulty in obtaining reference images in practical applications, and it will be the main direction of development of the objective IQA in the future [27]–[32].

In general, the NR-IQA can be divided into application-specific assessment and general-purpose assessment [33]. The application-specific NR-IQA metrics are effective only for a certain distortion or only for a certain application, while the general-purpose NR-IQA metrics are suitable for any distortion and any occasion [30], [32]. Several general-purpose NR-IQA metrics have been developed in these years, which typically reformulate the IQA problem into a classification and regression problem. The regressors/classifiers are always trained using specific features, and the relevant features are either discovered via machine learning (ML) or specified by using natural-scene statistics (NSS), both of which require a large number of distortion-free images as a prerequisite. Consequently, there are still much desired in some cases for the application-specific NR-IQA. Common types of distortion include JPEG compression distortion, blur distortion, noise distortion, and so on. For compression distorted images, Suthaharan [34] proposed a corresponding assessment metric VSBAM to evaluate the degree of image distortion caused by the image compression. For fuzzy degenerated images, Ciancio *et al*. [35] applied various airspace image features and used neural network model to evaluate the blurred image. Bahrami and Kot [36] proposed the concept of maximum local variation (MLV) to quickly assess the degree of blur of the image. Ferzli and Karam [37] proposed the concept of just noticeable blur (JNB) to evaluate the degree of blur, and proposed an upgraded version CPBD [38]. For the image of contrast distortion, Fang *et al*. [39] built NSS models to evaluate the quality of a contrast-distorted image simply and effectively. Fang *et al*. [39] noticed the areas of maximum information and properly combined local and global considerations to evaluate the contrast-distorted images. As we know, noise is an important factor in image distortion, but there is few studies proposing NR objective assessment metric dedicated to noise-distorted image. This paper is devoted to the study of NR-IQA for noise-distorted images.

Empirical mode decomposition (EMD) is a signal processing method for non-stationary signal analysis proposed by Huang *et al*. [40]. It can clearly distinguish the intrinsic mode functions (IMFs) of overlapping complex data without presetting the basis function as a wavelet decomposition. As long as the boundary conditions and termination criteria are dealt with properly, we can decompose the image in the scale from small to large, which is more convenient and easier than the wavelet implementation [41]. Nunes *et al*. [42] extended the one-dimensional EMD and proposed the bidimensional empirical mode decomposition (BEMD) for bidimensional application. The image components obtained by BEMD are within different frequency bands, and the human visual system (HVS) has different sensitivities to image components in different frequencies. Therefore, when reconstructing the image, in order to make the performance of the metric closer to the human eyes, we weight and sum the image components through the visual contrast sensitivity function (CSF).

In addition, with the in-depth study of the IMF's local feature analysis using Riesz transform [43], Riesz transform has been widely used in various image processing applications. Considering the effect of BEMD on noise deduction when combined with Riesz transform [44], we propose a NR-IQA for noise-distorted images. We use the Riesz transform feature maps of the image to be measured and the denoised image to calculate the similarity index. Since the IMFs of the image reflect the different frequency characteristics, we propose the concept of *Frequency Mapping* (FM) to combine the BEMD and HVS, which improves the assessment performance of the metric.

Experimental results on three public databases show that the proposed FMIQA evaluates the noise-distorted image in consistency with subjective assessment and can obtain better performance in image quality prediction than some of the FR-IQA metrics and most NR-IQA metrics mentioned in this paper. In addition, in the case of highly distorted images the proposed FMIQA keeps good monotonicity while state-of-the-art metrics (such as BLIINDSII [45] and FRIQUEE [46]) do not vary with the differential mean opinion scores (DMOS). It is worth mentioning that the implementation of the metric does not require training. This makes the good performance of the metric is universal in the evaluation of images, rather than only for certain databases.

The remaining contents of this paper are organized as follows: Section II introduces the metric block diagram and the calculation process. Section III proposes the concept of FM. Section IV presents the experimental results and the corresponding analysis. Section V concludes this paper.

II. THE PROPOSED FRAMEWORK

In this paper, the block diagram of the proposed FMIQA index based on frequency mapping is shown in Fig. 1. The Riesz transform feature maps of the denoised image g is obtained by performing BEMD and Riesz transform on the image f to be measured. Then it is compared with the Riesz transform feature maps of the noise distorted image f to get the final IQA score.

The noise-distorted image f is decomposed by BEMD to obtain four IMF components ($IMF1$, $IMF2$, $IMF3$, and $RESIDUE$), and five groups of Riesz transform feature maps are obtained by performing first and second order Riesz transform [47] on each image component (each group of feature maps contains four image components, the main frequencies of which are different).

Visual psychologists have pointed out that the contrast sensitivity of the HVS to different spatial frequencies is different. The human visual contrast sensitivity is a function of the spatial frequency and has the characteristics of a bandpass filter. In order to make the final assessment result closer to the subjective perception, we use the CSF to weight and sum the four image components in every group to obtain the feature

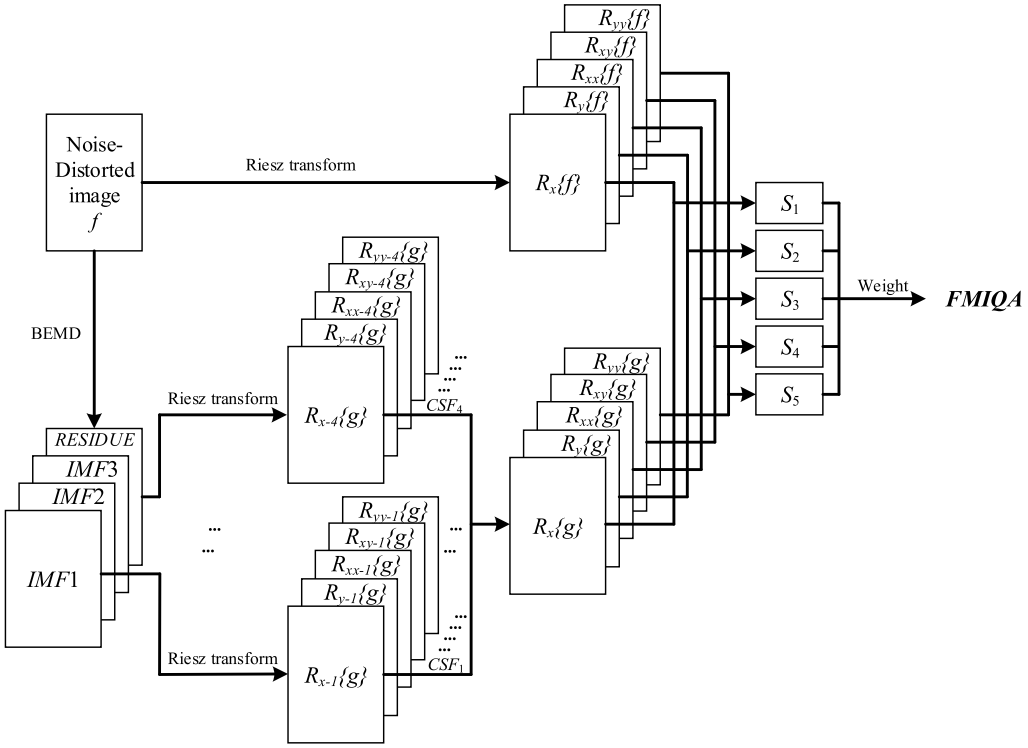

FIGURE 1. Illustration of the proposed FMIQA index.

maps $R_x\{g\}$, $R_y\{g\}$, $R_{xx}\{g\}$, $R_{xy}\{g\}$, and $R_{yy}\{g\}$, which are denoted as g_1, g_2, g_3, g_4, and g_5, respectively. At the same time, we perform the first and second order Riesz transform on the noise distorted image f and obtain the five feature maps $R_x\{f\}$, $R_y\{f\}$, $R_{xx}\{f\}$, $R_{xy}\{f\}$, and $R_{yy}\{f\}$ which are denoted as f_1, f_2, f_3, f_4, and f_5, respectively.

For the five groups corresponding feature maps $\{f_i, g_i\}$ $(i = 1, 2, \ldots, 5)$, the similarity is calculated as follows:

$$s_i(x, y) = \frac{2f_i(x, y)g_i(x, y) + C_i}{{f_i}^2(x, y) + {g_i}^2(x, y) + C_i} \tag{1}$$

where $f_i(x, y)$ and $g_i(x, y)$ are pixel values of the feature maps f_i and g_i at pixel (x, y), respectively. $s_i(x, y)$ is the similarity value of f_i and g_i $(i = 1, 2, \ldots, 5)$ at pixel (x, y). C_i $(i = 1, 2, \ldots, 5)$ denotes small positive value to avoid the instability caused by the denominator being zero or close to zero. In this paper, we take $C_i = 0.01$ $(i = 1, 2, \ldots, 5)$.

After obtaining the five similarity maps, we average the elements of the matrix to obtain five similarity indices:

$$S_i = \frac{\sum_{x=1}^{M}\sum_{y=1}^{N} s_i(x, y)}{M \times N} \tag{2}$$

where S_i $(i = 1, 2, \ldots, 5)$ denotes the similarity index of the feature maps f_i and g_i.

Finally, the five similarity indices are weighted and summed as the final IQA score:

$$FMIQA = \frac{\sum_{i=1}^{5} w_i \cdot S_i}{\sum_{i=1}^{5} w_i} \tag{3}$$

III. FREQUENCY MAPPING

BEMD has the advantages of smoothing irregular amplitude, weakening data singularity, and so on. After BEMD, the image is decomposed into a series of "fine to coarse" detailed information and a large-scale trend information according to the scale from small to large [48]. As the feature scale parameter is the actually measured data, the components obtained by the above method have obvious physical meaning, which characterizes the fluctuation condition and frequency range of the signal on a certain feature scale parameter [49].

We perform BEMD on two reference images selected from LIVE database [50]. The *buildings* contains rich high-frequency information, and the *caps* contains rich low-frequency information. We obtain *IMF*1, *IMF*2, *IMF*3, and *RESIDUE* of these two images. Then we do the spectral analysis on them and the results are shown in Fig. 2.

In Fig. 2, the *IMF*1 component mainly contains small-scale components, which reflect the finest details of the original image, that is, the high-frequency information. The *IMF*2 component mainly contains sub-scale components, and so on. The *RESIDUE* component mainly contains the remaining large-scale components, which reflects the contour information of the original image, that is, the low-frequency information. The detailed information describes the components of small scale in the image, like texture etc. and the remaining components of larger scale express the basic structure and the change trend of the image. We process the information

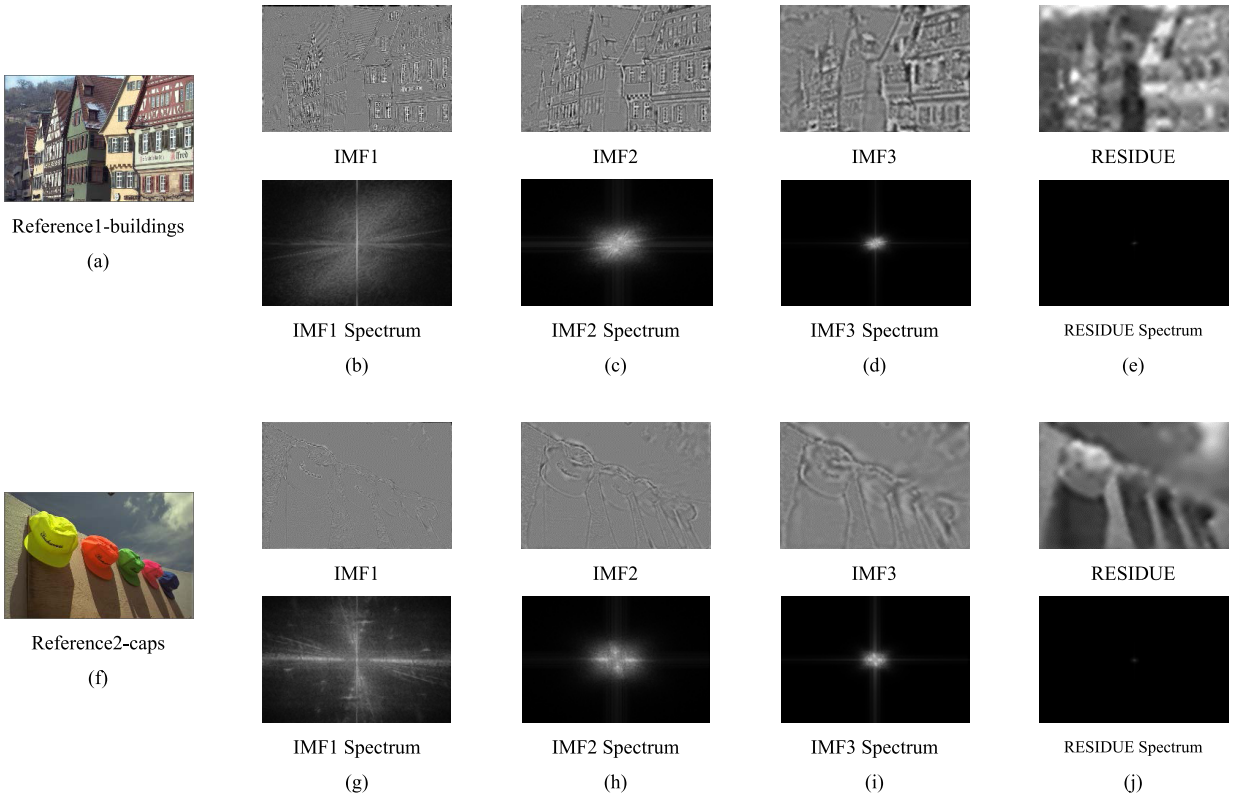

FIGURE 2. Two examples of BEMD. From left to right, top to bottom are the (a) reference image1-*buildings*, (b) IMF1 and its spectrum map, (c) IMF2 and its spectrum map, (d) IMF3 and its spectrum map, (e) RESIDUE and its spectrum map, (f) reference image2-*caps*, (g) IMF1 and its spectrum map, (h) IMF2 and its spectrum map, (i) IMF3 and its spectrum map, and (j) RESIDUE and its spectrum map.

of different scales thoroughly, and then the processing results in different scales are obtained.

We use the Riesz transform to get the local feature analysis on different scale information.

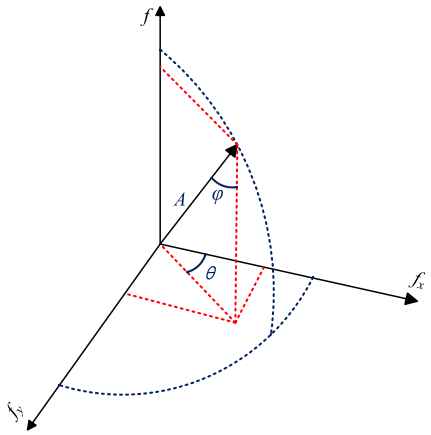

FIGURE 3. Riesz transform space. f, f_x, f_y are the projections of the points in the space on the three axes of the spherical coordinate system. $A(x, y)$, $\theta(x, y)$, $\varphi(x, y)$ are the local amplitude, the local direction, and the local phase.

In Fig. 3, f, f_x, f_y are the projections of the points in the space on the three axes of the spherical coordinate system. $A(x, y)$, $\theta(x, y)$, $\varphi(x, y)$ are the local amplitude, the local direction, and the local phase.

Using the first-order Riesz transform, we can extract the local linear features of the image, but we can not express the corner points and intersection points in the image [51]. In order to characterize various low-level features existing in the image, it is necessary to use higher order Riesz transform. In this paper, we use the second-order Riesz transform to express more complex features.

The first- and second-order Riesz transform can be used to extract the low-level features of the image *lighthouse*2 (image from the LIVE database [50]) to obtain five feature maps $R_x/R_y/R_{xx}/R_{xy}/R_{yy}$, as shown in Fig. 4. It can be seen from Fig. 4 that the first-order feature maps can express the edge contour of the image perfectly and the second-order feature maps can express more complex features such as corner points.

Five feature maps can be obtained for each image. In order to obtain the feature maps of the denoised image from the feature maps of different image components, we need to integrate different image components of each type of feature map. This paper uses the CSF proposed by Mannos and Sakrison [52] as the weighting. The formula of CSF is shown in Eq. (4), which reflects the difference in sensitivity of the HVS to different spatial frequencies.

$$A(f_r) \approx 2.6(0.0192 + 0.114f_r)\exp^{-(0.114f_r)^{1.1}} \tag{4}$$

where f_r is the spatial frequency.

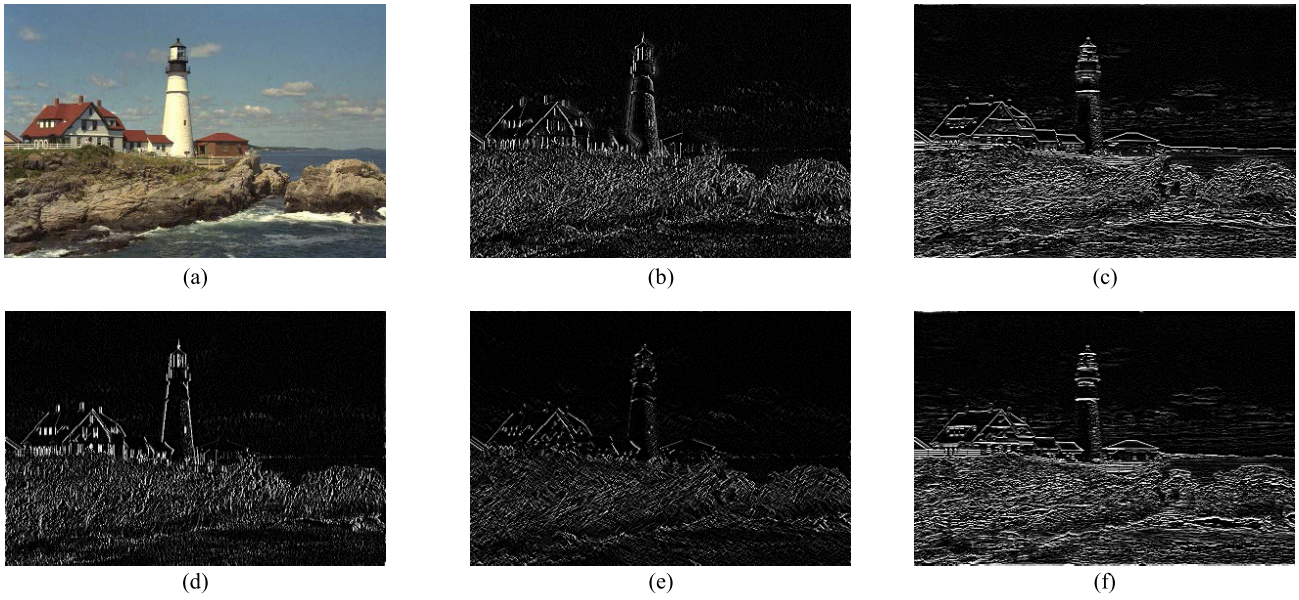

FIGURE 4. The first-order and second-order Riesz transform feature maps of the *lighthouse*2. From left to right and top to bottom are respectively the (a) *lighthouse*2, (b) R_x, (c) R_y, (d) R_{xx}, (e) R_{xy}, and (f) R_{yy}.

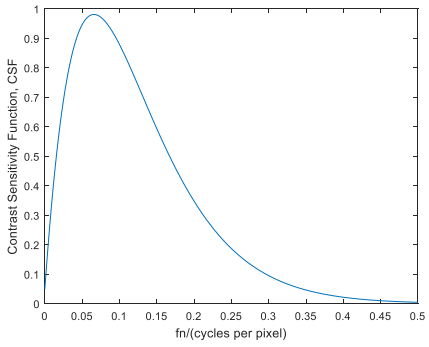

FIGURE 5. The curve of contrast sensitivity function. It reflects the difference in sensitivities of the HVS to different spatial frequencies.

According to Eq. (4), the feature curve of normalized CSF is shown in Fig. 5.

Fig. 5 shows that the contrast sensitivity of CSF curve is the largest at the intermediate frequency region, and the sensitivity is obviously decreased in the lower frequency and higher frequency region. There are four image components after BEMD: $IMF1$, $IMF2$, $IMF3$, and $RESIDUE$. The spatial frequency range of these four components is different, so their contrast sensitivities of the HVS are different.

When we weight and sum the Riesz transform feature maps in each group by the CSF values corresponding to the different image components, we find that when the frequency boundary of different image components is directly used as the characteristic frequency of the frequency band, the error is large. The frequency boundary of the $IMF1$ is high, and it has a great jump relative to the other lower frequency bands. In order to obtain more appropriate image boundary frequency information, we propose a new method: FM. Through the FM, we can find the new accurate frequency boundary of the image component, so as to find out the corresponding contrast sensitivity as the weight of the image component feature map.

The detailed steps of FM are shown as follows:

1) Perform BEMD on noise distorted image and obtain four image components: IMF1, IMF2, IMF3, and RESIDUE.
2) Compress the IMF's spectrum, as follows:

$$Compressed\ Spectrum = \frac{Spectrum}{m^{2\times\frac{f}{f_0}}} \tag{5}$$

where m is centered on 2, and f_0 generally does not exceed 0.5 (because the upper limit of the spatial frequency is 0.5). Specific values are determined by the experiment.
3) Integrate the $IMF1$ to obtain the volume V_{IMF} of the area between the scatter plot and the $x-y$ plane. With the origin as the center and the maximum value of IMF as height, we take the appropriate radius value for a cylinder, so that the cylinder volume $V = V_{IMF}$. The value of the radius is the boundary value of $IMF1$ frequency domain. Since the spectrum of the $IMF1$ is a scatter plot and has a certain randomness, we take the average of the IMF frequency domain boundary of multiple pictures as the characteristic frequency f_f^1 of the IMF frequency domain boundary.
4) Calculate the characteristic frequency f_f^i $(i = 2, 3, 4)$ by performing step 3) on $IMF2$, $IMF3$, and $RESIDUE$ in turn.
5) The CSF frequency f_c^i $(i = 1, 2, 3, 4)$ is obtained by mapping the characteristic frequency f_f^i $(i = 1, 2, 3, 4)$

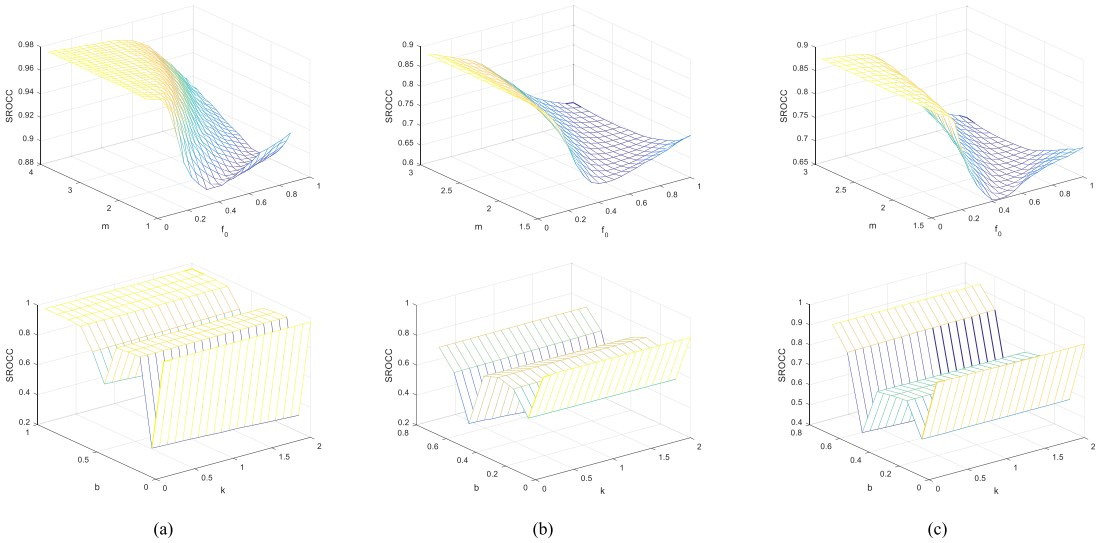

(a) (b) (c)

FIGURE 6. Orthogonal Experiments for FM Parameters. (a) Experimental results on LIVE database, (b) experimental results on CSIQ database, and (c) experimental results on TID2013 database.

according to the mapping relation as follows.

$$f_c^i = k \times f_f^i + b \tag{6}$$

where $i = 1, 2, 3, 4$. The two parameters k and b of the mapping relation are experimentally determined.

6) The contrast sensitivity of the HVS corresponding to f_c^i ($i = 1, 2, 3, 4$) is used as the weight A_i ($i = 1, 2, 3, 4$) of the image components. Thus, Eq. (4) becomes as follows:

$$A_i \approx 2.6[0.0192 + 0.114 f_c^i] \exp^{-(0.114 f_c^i)^{1.1}} \tag{7}$$

where $i = 1, 2, 3, 4$.

In this way, the correspondence between the image components and the HVS is obtained.

IV. EXPERIMENTAL RESULTS

This paper performs performance comparison on three image databases LIVE [50], CSIQ [53] and TID2013 [54]. LIVE database contains 29 reference images and 779 distorted images. The distortion types include JPEG2000, JPEG compression, white noise, Gaussian blur, and Rayleigh fading. The database provides the DMOS for each image. The smaller DMOS value represents higher image quality. CSIQ database contains 30 reference images, each of which has 6 types of distortion, each with four or five levels. The database provides the DMOS values for all images, the value range of which in the database is [0, 1]. TID2013 database includes 25 colored reference images, and there are 24 types of distortion, totaling 3000 images. Mean opinion scores (MOS) values of all tested images and their standard deviation are obtained by the statistics of subjective scores from 971 participants of different countries. Since FMIQA is designed for noise-distorted images only, we select only part of the images in three databases for experiments, including white noise (174 images) in LIVE database, additive white gaussian noise (150 images) in CSIQ database, and high frequency noise (125 images) in TID2013 database.

In this paper, we use the five-parameter nonlinear logistic regression function to fit the data [55]. The subjective scores are predicted by the following regression.

$$f(x) = \beta_1 [\frac{1}{2} - \frac{1}{1 + \exp(\beta_2 (x - \beta_3))}] + \beta_4 x + \beta_5 \tag{8}$$

where x is the objective IQA score; $f(x)$ is the IQA prediction score; β_1, β_2, β_3, β_4, and β_5 are regressing function parameters.

A. DETERMINATION OF PARAMETERS

There are several parameters need to be determined for FMIQA: the FM Parameters, the screening termination condition parameter, and the similarity index weight parameters. The FM Parameters are determined by orthogonal experiments, the screening termination condition parameter is determined by traversal experiment, and the similarity index weight parameters are determined by fitting the similarity indices with DMOS. Although these parameters are determined on these three databases, it should be noted that once these parameters are determined, they are fixed for all the following experiments conducted, and are not related to a specific database.

1) DETERMINATION OF FM PARAMETERS

In the process of FM, we have four parameters to be determined, which are m, f_0, k, and b. Since m and f_0 are interrelated, and k and b are interrelated, we perform orthogonal experiments on m and f_0, and k and b on three databases. We use the Spearman Rank-Order Correlation Coefficient (SROCC) to evaluate the performance of the objective assessment [56]. The relationship between parameters and performance index SROCC is shown in Fig. 6. Fig. 6 shows

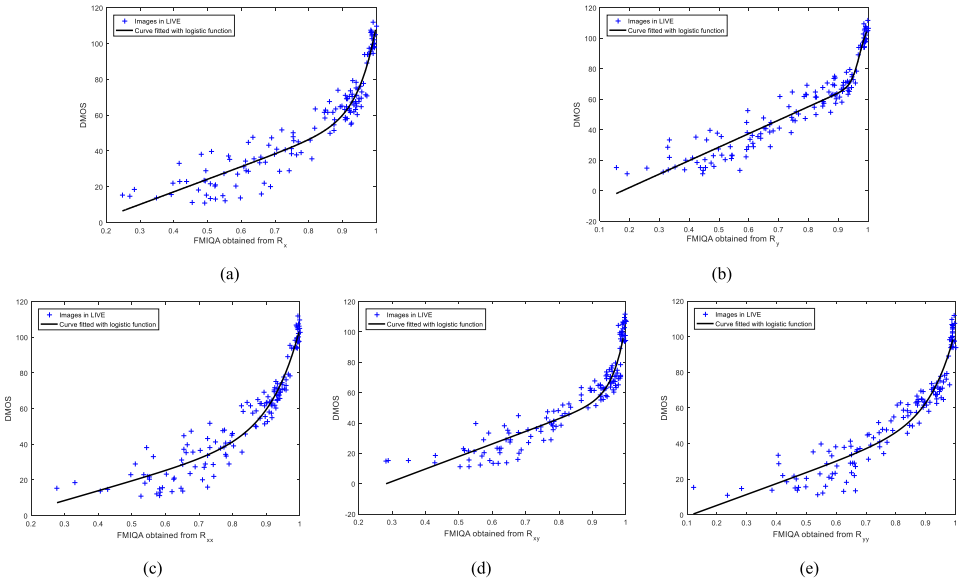

FIGURE 7. Fitting the similarity indices with DMOS. (a) *FMIQA* obtained using R_x, *SROCC* = 0.9487, (b) *FMIQA* obtained using R_y, *SROCC* = 0.9581, (c) *FMIQA* obtained using R_{xx}, *SROCC* = 0.9598, (d) *FMIQA* obtained using R_{xy}, *SROCC* = 0.9587, and (e) *FMIQA* obtained using R_{yy}, *SROCC* = 0.9636.

that the performance of these parameters in different databases is slightly different, but the difference is very small. In order to make the metric more universal, we have made a compromise on the determination of the parameters on different databases, and finally we set $m = 3$, $f_0 = 0.05$, $k = 0.4$, and $b = 0$.

TABLE 1. SROCC/RMSE values comparison with different screening termination condition parameter *SD* on LIVE database.

SD	SROCC	RMSE
0.20	0.9746	5.7597
0.22	0.9746	5.7562
0.24	0.9746	5.7545
0.26	0.9746	5.7543
0.28	0.9746	5.7535
0.30	0.9746	5.7535

2) DETERMINATION OF THE SCREENING TERMINATION CONDITION PARAMETER

When we perform the BEMD, the value of the screening termination condition parameter *SD* needs to be determined. The criterion for the termination of the screening process is a theoretical criterion similar to the Cauchy convergence criterion, which usually sets the value of *SD* between 0.2 and 0.3. That is, the screening process can be completed when *SD* is less than the threshold [57]. In this paper, we set $SD = 0.3$. To verify the rationality of this parameter selection, we compare the performance of the metric by SROCC and Root Mean Squared Error (RMSE). In Table 1 we list the *SROCC*/*RMSE* performance indices obtained by applying the FMIQA index to the LIVE database when different *SD* is taken. Table 1 indicates that the performance of the metric is not sensitive to the SD value. In particular, when SD is between 0.28 and 0.30, the performance is no longer optimized. At the same time, the greater the *SD*, the less the number of screening, and the faster the screening rate. Therefore, we set *SD* as 0.3, taking performance and efficiency of the metric into account.

3) DETERMINATION OF SIMILARITY INDEX WEIGHT

In the experiment, we fit the similarity indices S_i $(i = 1, 2, \ldots, 5)$ of each feature map with DMOS, and get five scatter plots, as shown in Fig. 7.

Fig. 7 shows that the *SROCC* values obtained by fitting the DMOS and the similarity indices are different. We use $SROCC_i$ $(i = 1, 2, \ldots, 5)$ as the weight of the similarity indices S_i $(i = 1, 2, \ldots, 5)$, that is, $w_i = SROCC_i$ $(i = 1, 2, \ldots, 5)$. Eq. (3) can be defined as:

$$FMIQA = \frac{\sum_{i=1}^{5} SROCC_i \cdot S_i}{\sum_{i=1}^{5} SROCC_i} \tag{9}$$

where $SROCC_i$ $(i = 1, 2, 3, 4, 5)$ are determined as: $SROCC_1 = 0.9487$, $SROCC_2 = 0.9581$, $SROCC_3 = 0.9598$, $SROCC_4 = 0.9587$, and $SROCC_5 = 0.9636$.

B. PERFORMANCE ANALYSIS

1) COMPARISON OF INDICES

Table 2 lists the *SROCC* values of FMIQA index and other FR- and NR-IQA metrics for noise-distorted images on the LIVE, CSIQ, and TID2013 databases, where PSNR, SSIM [16], GMSD [58], GSSIM [59], MS-SSIM [60], RFSIM [51], and FSIM [61] are classical FR-IQA metrics, BLIINDSII [45], FRIQUEE [46], CORNIA [62], NIQE [63], QAC [64], IL-NIQE [65], and FMIQA proposed in this paper

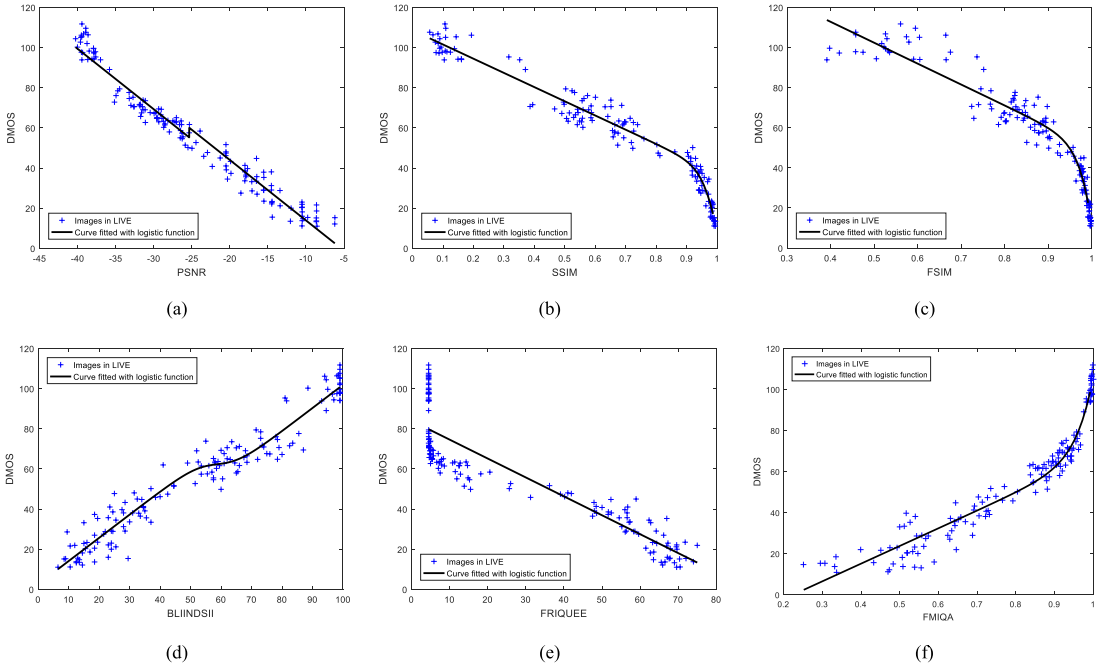

FIGURE 8. Scatter plots of predicted quality scores on LIVE database. From left to right, top to bottom are the (a) PSNR, (b) SSIM, (c) FSIM, (d) BLIINDSII, (e) FRIQUEE, and (f) FMIQA.

TABLE 2. SROCC of different metrics for noise-distorted images on different databases (Italicized metrics are NR-IQA metrics; others are FR-IQA metrics).

Model	LIVE	CSIQ	TID2013	Average
PSNR	0.985	0.936	0.914	0.945
SSIM [16]	0.964	0.897	0.863	0.908
FSIM [61]	0.965	0.926	0.897	0.929
GMSD [58]	0.974	0.968	0.916	0.953
GSSIM [59]	0.933	0.830	0.753	0.839
MS-SSIM [60]	0.973	0.947	0.860	0.927
RFSIM [51]	0.980	0.940	0.914	0.945
BLIINDSII [45]	0.960	0.801	0.825	0.862
FRIQUEE [46]	**0.982**	**0.854**	**0.900**	**0.912**
CORNIA [62]	0.936	0.746	0.796	0.826
NIQE [63]	0.972	0.810	0.845	0.876
QAC [64]	0.951	0.822	0.863	0.879
IL-NIQE [65]	**0.981**	**0.850**	**0.869**	**0.900**
FMIQA	**0.975**	**0.877**	**0.874**	**0.909**

are NR-IQA metrics. The top three performance NR-IQA indices are highlighted in bold. We can see that, FMIQA index has good performance on all three databases, which performs better than some of the FR-IQA metrics and most NR-IQA metrics mentioned in this paper. Results of CORNIA [62] and QAC [64] are taken from the original papers.

Fig. 8 shows the scatter plots of six different IQA metrics for noise distorted images in LIVE database. It is easy to see that BLIINDSII [45] and FRIQUEE [46] are not monotonic when the image is highly distorted (DMOS is about 80 $\sim$ 110), and the scatter plot fitted by FMIQA index is evenly distributed in the whole coordinate system and has a strong linear relationship with DMOS, which further proves the robust performance of FMIQA index.

2) STABILITY TEST

A stable NR-IQA metric should be a monotonic function of the image distortion level. However, when the degree of distortion is high, some of the metrics lose stability, such as BLIINDSII [45] and FRIQUEE [46]. In order to compare the stability between the proposed FMIQA and other NR-IQA metrics, we select 6 noise-distorted images from the LIVE database. Fig. 9a, 9b, 9c, 9d, 9e, 9f are noise-distorted images in different degrees, the DMOS values of which are different. We calculate the objective values of the distorted images using FMIQA and other metrics. The results can be found in Fig. 9.

Assessment results indicate that when the degree of distortion is high, the BLIINDSII and FRIQUEE metrics are no longer monotonic, and the scores of the images with different DMOS values are the same. However, when the degree of distortion is high, FMIQA still has the monotonicity and with the larger DMOS value, the higher the IQA score, which means the higher degree of distortion. Consequently, FMIQA is more stable than the NR-IQA metrics BLIINDSII and FRIQUEE mentioned in this paper.

In order to illustrate the stability of the metric more intuitively, we plot the function curves between DMOS and BLIINDSII, FRIQUEE, and FMIQA according to Fig. 9.

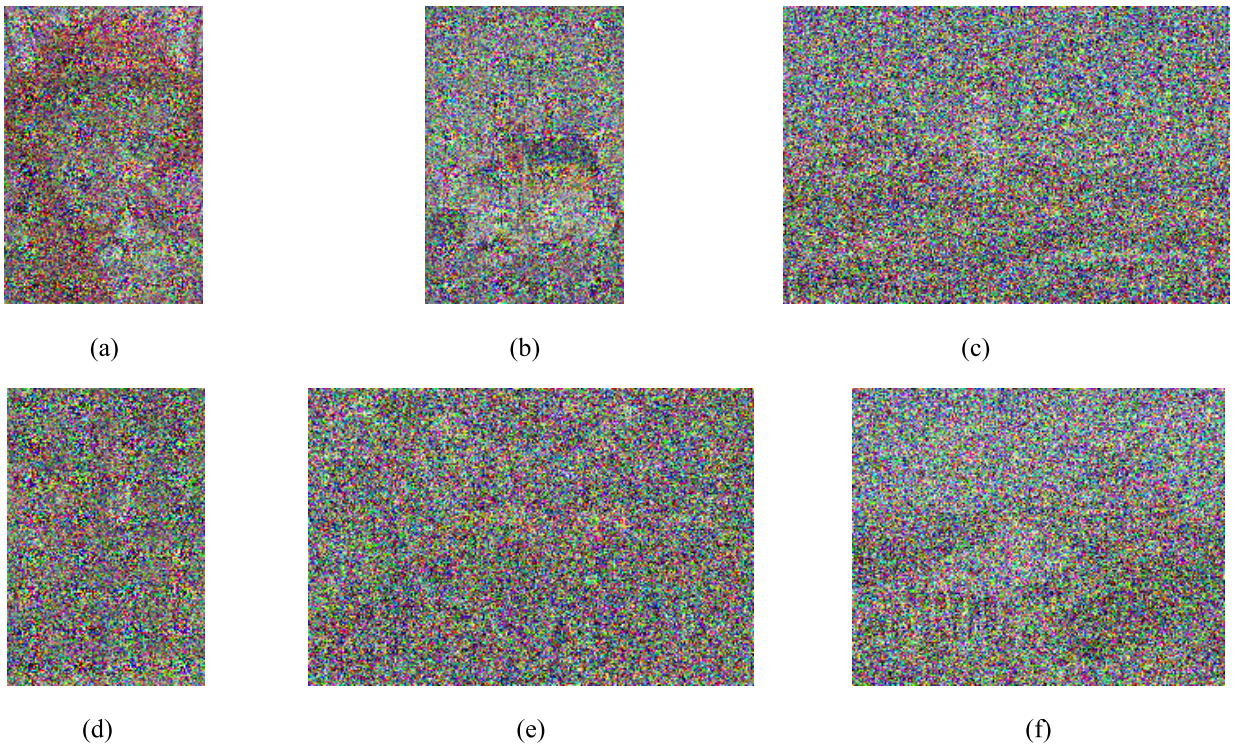

FIGURE 9. Stability test results on LIVE database. (a) img60, DMOS = 97.6570, BLIINDSII = 99, FRIQUEE = 4.981, FMIQA = 0.9870, (b) img113, DMOS = 97.9247, BLIINDSII = 99, FRIQUEE = 4.981, FMIQA = 0.9876, (c) img137, DMOS = 102.0154, BLIINDSII = 99, FRIQUEE = 4.981, FMIQA = 0.9892, (d) img33, DMOS = 102.7237, BLIINDSII = 99, FRIQUEE = 4.981, FMIQA = 0.9905, (e) img87, DMOS = 105.1017, BLIINDSII = 99, FRIQUEE = 4.981, FMIQA = 0.9911, and (f) img20, DMOS = 111.7747, BLIINDSII = 99, FRIQUEE = 4.981, FMIQA = 0.9955.

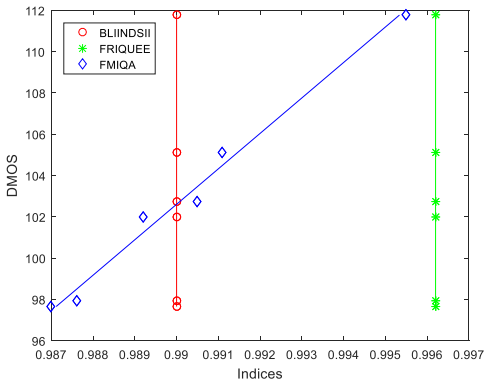

FIGURE 10. The function curves between DMOS and BLIINDSII, FRIQUEE, and FMIQA according to Fig. 9. In the case of highly distorted images, the proposed FMIQA keeps good monotonicity while BLIINDSII and FRIQUEE does not vary with the DMOS.

As shown in Fig. 10 (the BLIINDSII and FRIQUEE indices are normalized), in the case of highly distorted images, the proposed FMIQA keeps good monotonicity while BLIINDSII and FRIQUEE do not vary with the DMOS. It validates that FMIQA achieves good prediction performance.

V. CONCLUSIONS

IQA for noise-distorted images is an important problem in the field of image processing analysis. In this paper, an effective and novel NR-IQA metric for assessing noise-distorted images named FMIQA index is proposed. FMIQA combines BEMD and Riesz transform with appropriate application of CSF curve, which takes the sensitive features of HVS into account. In order to obtain more accurate image boundary frequency information, we propose a new method: frequency mapping. The metric is tested on LIVE, CSIQ, and TID2013 databases. The scatter plots and stability test experiments are carried out on LIVE database. The experimental results show that the FMIQA index has good performance in assessing the noise-distorted images.

ACKNOWLEDGMENT

The authors would like to thank Dr. Han Hu, Prof. Yuming Fang, and Prof. Hao Jiang for the valuable opinions they have offered.

REFERENCES

[1] Z. Wang, "Applications of objective image quality assessment methods [applications corner]," *IEEE Signal Process. Mag.*, vol. 28, no. 6, pp. 137–142, Nov. 2011.

[2] Y. Fang, J. Yan, J. Liu, S. Wang, Q. Li, and Z. Guo, "Objective quality assessment of screen content images by uncertainty weighting," *IEEE Trans. Image Process.*, vol. 26, no. 4, pp. 2016–2027, Apr. 2017.

[3] J. Ma, Y. Ma, J. Zhao, and J. Tian, "Image feature matching via progressive vector field consensus," *IEEE Signal Process. Lett.*, vol. 22, no. 6, pp. 767–771, Jun. 2015.

[4] Y. Fang, K. Zeng, Z. Wang, W. Lin, Z. Fang, and C.-W. Lin, "Objective quality assessment for image retargeting based on structural similarity," *IEEE J. Emerg. Sel. Topics Circuits Syst.*, vol. 4, no. 1, pp. 95–105, Mar. 2014.

[5] C. Yang, J. Ma, M. Zhang, S. Zheng, and X. Tian, "Multiscale facet model for infrared small target detection," *Infr. Phys. Technol.*, vol. 67, pp. 202–209, Nov. 2014.
[6] C. Zhou, H. Jiang, Y. Chen, L. Wu, and S. Yi, "User interest acquisition by adding home and work related contexts on mobile big data analysis," in *Proc. IEEE Conf. Comput. Commun. Workshops (INFOCOM WKSHPS)*, Apr. 2016, pp. 201–206.
[7] H. Hu, Y. Wen, and D. Niyato, "Public cloud storage-assisted mobile social video sharing: A supermodular game approach," *IEEE J. Sel. Areas Commun.*, vol. 35, no. 3, pp. 545–556, Mar. 2017.
[8] K. Gu, G. Zhai, X. Yang, W. Zhang, and M. Liu, "Subjective and objective quality assessment for images with contrast change," in *Proc. IEEE Int. Conf. Image Process.*, Dec. 2013, pp. 383–387.
[9] W. Lin and C.-C. Jay Kuo, "Perceptual visual quality metrics: A survey," *J. Vis. Commun. Image Represent.*, vol. 22, no. 4, pp. 297–312, 2011.
[10] H. Yang, Y. Fang, W. Lin, and Z. Wang, "Subjective quality assessment of screen content images," in *Proc. 6th Int. Workshop Quality Multimedia Exper. (QoMEX)*, 2014, pp. 257–262.
[11] K. Seshadrinathan, R. Soundararajan, A. C. Bovik, and L. K. Cormack, "Study of subjective and objective quality assessment of video," *IEEE Trans. Image Process.*, vol. 19, no. 6, pp. 1427–1441, Jun. 2010.
[12] Z. Wang and A. C. Bovik, "Modern image quality assessment," *Synthesis Lectures Image, Video, Multimedia Process.*, vol. 2, no. 1, pp. 1–156, Jan. 2006.
[13] Z. Wang, A. C. Bovik, and L. Lu, "Why is image quality assessment so difficult?" in *Proc. IEEE Int. Conf. Acoust., Speech, Signal Process. (ICASSP)*, vol. 4. May 2002, p. IV–3313.
[14] H.-J. Park and D.-H. Har, "Subjective image quality assessment based on objective image quality measurement factors," *IEEE Trans. Consum. Electron.*, vol. 57, no. 3, pp. 1176–1184, Aug. 2011.
[15] M. Cheon and J.-S. Lee, "On ambiguity of objective image quality assessment," *Electron. Lett.*, vol. 52, no. 1, pp. 34–35, 2015.
[16] Z. Wang, A. C. Bovik, H. R. Sheikh, and E. P. Simoncelli, "Image quality assessment: From error visibility to structural similarity," *IEEE Trans. Image Process.*, vol. 13, no. 4, pp. 600–612, Apr. 2004.
[17] L. Zhang, L. Zhang, X. Mou, and D. Zhang, "A comprehensive evaluation of full reference image quality assessment algorithms," in *Proc. 19th IEEE Int. Conf. Image Process.*, Sep. 2012, pp. 1477–1480.
[18] Y. Ding, S. Wang, and D. Zhang, "Full-reference image quality assessment using statistical local correlation," *Electron. Lett.*, vol. 50, no. 2, p. 79, 2014.
[19] S.-H. Bae and M. Kim, "A novel image quality assessment with globally and locally consilient visual quality perception," *IEEE Trans. Image Process.*, vol. 25, no. 5, pp. 2392–2406, May 2016.
[20] K. Gu *et al.*, "Saliency-guided quality assessment of screen content images," *IEEE Trans. Multimedia*, vol. 18, no. 6, pp. 1098–1110, Jun. 2016.
[21] Q. Li and Z. Wang, "Reduced-reference image quality assessment using divisive normalization-based image representation," *IEEE J. Sel. Topics Signal Process.*, vol. 3, no. 2, pp. 202–211, Apr. 2009.
[22] A. Rehman and Z. Wang, "Reduced-reference image quality assessment by structural similarity estimation," *IEEE Trans. Image Process.*, vol. 21, no. 8, pp. 3378–3389, Aug. 2012.
[23] Z. Wang and A. C. Bovik, "Reduced- and no-reference image quality assessment," *IEEE Signal Process. Mag.*, vol. 28, no. 6, pp. 29–40, Nov. 2011.
[24] J. Wu, W. Lin, G. Shi, and A. Liu, "Reduced-reference image quality assessment with visual information fidelity," *IEEE Trans. Multimedia*, vol. 15, no. 7, pp. 1700–1705, Nov. 2013.
[25] J. Farah, M.-R. Hojeij, J. Chrabieh, and F. Dufaux, "Full-reference and reduced-reference quality metrics based on SIFT," in *Proc. IEEE Int. Conf. Acoust., Speech Signal Process. (ICASSP)*, May 2014, pp. 161–165.
[26] M. Liu, K. Gu, G. Zhai, P. Le Callet, and W. Zhang, "Perceptual reduced-reference visual quality assessment for contrast alteration," *IEEE Trans. Broadcast.*, vol. 63, no. 1, pp. 71–81, Mar. 2017.
[27] A. K. Moorthy and A. C. Bovik, "Blind image quality assessment: From natural scene statistics to perceptual quality," *IEEE Trans. Image Process.*, vol. 20, no. 12, pp. 3350–3364, Dec. 2011.
[28] P. Ye and D. Doermann, "No-reference image quality assessment using visual codebooks," *IEEE Trans. Image Process.*, vol. 21, no. 7, pp. 3129–3138, Jul. 2012.
[29] K. Gu, G. Zhai, W. Lin, X. Yang, and W. Zhang, "No-reference image sharpness assessment in autoregressive parameter space," *IEEE Trans. Image Process.*, vol. 24, no. 10, pp. 3218–3231, Oct. 2015.
[30] V. Kamble and K. Bhurchandi, "No-reference image quality assessment algorithms: A survey," *Opt.-Int. J. Light Electron Opt.*, vol. 126, no. 11, pp. 1090–1097, 2015.
[31] R. Fang, R. Al-Bayaty, and D. Wu, "Bnb method for no-reference image quality assessment," *IEEE Trans. Circuits Syst. Video Technol.*, vol. 27, no. 7, pp. 1381–1391, Jul. 2016.
[32] S. Xu, S. Jiang, and W. Min, "No-reference/blind image quality assessment: A survey," *IETE Tech. Rev.*, vol. 34, no. 3, pp. 223–245, 2016.
[33] D. M. Chandler, "Seven challenges in image quality assessment: Past, present, and future research," *ISRN Signal Process.*, vol. 2013, pp. 1–53, Feb. 2013.
[34] S. Suthaharan, "No-reference visually significant blocking artifact metric for natural scene images," *Signal Process.*, vol. 89, no. 8, pp. 1647–1652, 2009.
[35] A. Ciancio, A. L. N. T. da Costa, E. A. B. da Silva, A. Said, R. Samadani, and P. Obrador, "No-reference blur assessment of digital pictures based on multifeature classifiers," *IEEE Trans. Image Process.*, vol. 20, no. 1, pp. 64–75, Jan. 2011.
[36] K. Bahrami and A. C. Kot, "A fast approach for no-reference image sharpness assessment based on maximum local variation," *IEEE Signal Process. Lett.*, vol. 21, no. 6, pp. 751–755, Jun. 2014.
[37] R. Ferzli and L. J. Karam, "A no-reference objective image sharpness metric based on the notion of just noticeable blur (JNB)," *IEEE Trans. Image Process.*, vol. 18, no. 4, pp. 717–728, Apr. 2009.
[38] N. D. Narvekar and L. J. Karam, "A no-reference image blur metric based on the cumulative probability of blur detection (CPBD)," *IEEE Trans. Image Process.*, vol. 20, no. 9, pp. 2678–2683, Sep. 2011.
[39] Y. Fang, K. Ma, Z. Wang, W. Lin, Z. Fang, and G. Zhai, "No-reference quality assessment of contrast-distorted images based on natural scene statistics," *IEEE Signal Process. Lett.*, vol. 22, no. 7, pp. 838–842, Jul. 2015.
[40] N. E. Huang *et al.*, "The empirical mode decomposition and the Hilbert spectrum for nonlinear and non-stationary time series analysis," *Proc. Roy. Soc. London Ser. A, Math., Phys. Eng. Sci.*, vol. 454, no. 1971, pp. 903–995, Mar. 1998.
[41] Z. Wu, N. E. Huang, and X. Chen, "The multi-dimensional ensemble empirical mode decomposition method," *Adv. Adapt. Data Anal.*, vol. 1, no. 3, pp. 339–372, 2009.
[42] J. C. Nunes, Y. Bouaoune, E. Delechelle, O. Niang, and P. Bunel, "Image analysis by bidimensional empirical mode decomposition," *Image Vis. Comput.*, vol. 21, no. 12, pp. 1019–1026, 2003.
[43] P. Cerejeiras and U. Kähler, "Monogenic signal theory," *Oper. Theory*, vol. 21, pp. 1701–1724, 2015.
[44] P. Flandrin, G. Rilling, and P. Goncalves, "Empirical mode decomposition as a filter bank," *IEEE Signal Process. Lett.*, vol. 11, no. 2, pp. 112–114, Feb. 2004.
[45] M. A. Saad, A. C. Bovik, and C. Charrier, "Blind image quality assessment: A natural scene statistics approach in the DCT domain," *IEEE Trans. Image Process.*, vol. 21, no. 8, pp. 3339–3352, Aug. 2012.
[46] D. Ghadiyaram and A. C. Bovik. (2016). "Perceptual quality prediction on authentically distorted images using a bag of features approach." [Online]. Available: https://arxiv.org/abs/1609.04757
[47] X.-G. Luo, H.-J. Wang, and S. Wang, "Monogenic signal theory based feature similarity index for image quality assessment," *AEU-Int. J. Electron. Commun.*, vol. 69, no. 1, pp. 75–81, 2015.
[48] S. R. Long, "Applications of hht in image analysis," in *Hilbert–Huang Transform and Its Applications*. Singapore: World Scientific, 2005, pp. 289–305.
[49] J. Wan, L. Ren, and C. Zhao, "Image feature extraction based on the two-dimensional empirical mode decomposition," in *Proc. Congr. Image Signal Process. (CISP)*, vol. 1. 2008, pp. 627–631.
[50] H. R. Sheikh, Z. Wang, L. Cormack, and A. C. Bovik, *LIVE Image Quality Assessment Database Release 2*. [Online]. Available: http://live.ece.utexas.edu/research/quality
[51] L. Zhang, L. Zhang, and X. Mou, "RFSIM: A feature based image quality assessment metric using riesz transforms," in *Proc. 17th IEEE Int. Conf. Image Process. (ICIP)*, Dec. 2010, pp. 321–324.
[52] J. Mannos and D. J. Sakrison, "The effects of a visual fidelity criterion of the encoding of images," *IEEE Trans. Inf. Theory*, vol. 20, no. 4, pp. 525–536, Jul. 1974.
[53] E. C. Larson and D. M. Chandler, "Most apparent distortion: Full-reference image quality assessment and the role of strategy," *J. Electron. Imag.*, vol. 19, no. 1, p. 011006, 2010.

[54] N. Ponomarenko *et al.*, "Image database TID2013: Peculiarities, results and perspectives," *Signal Process., Image Commun.*, vol. 30, pp. 57–77, Jan. 2015.
[55] H. R. Sheikh, M. F. Sabir, and A. C. Bovik, "A statistical evaluation of recent full reference image quality assessment algorithms," *IEEE Trans. Image Process.*, vol. 15, no. 11, pp. 3440–3451, Nov. 2006.
[56] P. Corriveau and A. Webster, "Final report from the video quality experts group on the validation of objective models of video quality assessment, phase II," Video Quality Experts Group, CO, USA, Tech. Rep. Phase II (FR_TV2), 2003.
[57] J. C. Nunes, O. Niang, Y. Bouaoune, E. Delechelle, and P. Bunel, "Bidimensional empirical mode decomposition modified for texture analysis," in *Proc. Scandin. Conf. Image Anal.*, 2003, pp. 171–177.
[58] W. Xue, L. Zhang, X. Mou, and A. C. Bovik, "Gradient magnitude similarity deviation: A highly efficient perceptual image quality index," *IEEE Trans. Image Process.*, vol. 23, no. 2, pp. 684–695, Feb. 2014.
[59] G.-H. Chen, C.-L. Yang, and S.-L. Xie, "Gradient-based structural similarity for image quality assessment," in *Proc. IEEE Int. Conf. Image Process.*, Dec. 2006, pp. 2929–2932.
[60] Z. Wang, E. P. Simoncelli, and A. C. Bovik, "Multiscale structural similarity for image quality assessment," in *Proc. 37th Asilomar Conf. Signals, Syst. Comput.*, vol. 2. Nov. 2003, pp. 1398–1402.
[61] L. Zhang, L. Zhang, X. Mou, and D. Zhang, "FSIM: A feature similarity index for image quality assessment," *IEEE Trans. Image Process.*, vol. 20, no. 8, pp. 2378–2386, Aug. 2011.
[62] P. Ye, J. Kumar, L. Kang, and D. Doermann, "Unsupervised feature learning framework for no-reference image quality assessment," in *Proc. IEEE Conf. Comput. Vis. Pattern Recognit. (CVPR)*, Jun. 2012, pp. 1098–1105.
[63] A. Mittal, R. Soundararajan, and A. C. Bovik, "Making a 'completely blind' image quality analyzer," *IEEE Signal Process. Lett.*, vol. 20, no. 3, pp. 209–212, Mar. 2013.
[64] W. Xue, L. Zhang, and X. Mou, "Learning without human scores for blind image quality assessment," in *Proc. IEEE Conf. Comput. Vis. Pattern Recognit.*, Jun. 2013, pp. 995–1002.
[65] L. Zhang, L. Zhang, and A. C. Bovik, "A feature-enriched completely blind image quality evaluator," *IEEE Trans. Image Process.*, vol. 24, no. 8, pp. 2579–2591, Aug. 2015.

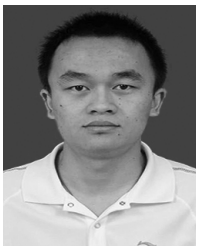

GUANGYI YANG received the M.Sc. degree in electronic engineering from Wuhan University, China, in 2008. He is currently an Engineer with the School of Electronic Information, Wuhan University.

His research interests involve in machine vision and image processing.

YUE LIAO is currently pursuing the B.Sc. degree with the School of Electronic Information, Wuhan University, China.

His research interests include image processing and robot vision.

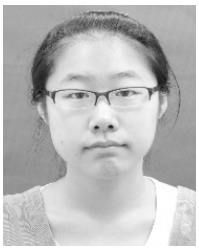

QINGYI ZHANG is currently pursuing the B.Sc. degree with the School of Electronic Information, Wuhan University, China.

Her research interests include image processing and computer vision.

DESHI LI received the Ph.D. degree in computer science from Wuhan University, China, in 2001. He is currently a Professor and the Dean of the School of Electronic Information, Wuhan University.

His research is involved in image processing, wireless sensor networks, networked robots, and wireless communication.

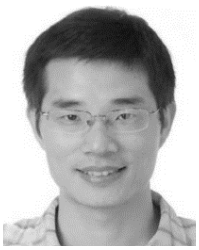

WEN YANG (M'09–SM'16) received the B.Sc. degree in electronic apparatus and surveying technology, the M.Sc. degree in computer application technology, and the Ph.D. degree in communication and information system, all from Wuhan University, Wuhan, China, in 1998, 2001, and 2004, respectively.

From 2008 to 2009, he was a Visiting Scholar with the Apprentissageet Interfaces Team, Laboratoire Jean Kuntzmann, Grenoble, France. From 2010 to 2013, he was a Post-Doctoral Researcher with the State Key Laboratory of Information Engineering in Surveying, Mapping and Remote Sensing, Wuhan University. He is currently a Full Professor with the School of Electronic Information, Wuhan University.

His research interests include object detection and recognition, image retrieval and semantic segmentation, multisensor information fusion, and change detection.